HHS Public Access

Author manuscript

IEEE Trans Ultrason Ferroelectr Freq Control. Author manuscript; available in PMC 2022 June 01.

Published in final edited form as:

IEEE Trans Ultrason Ferroelectr Freq Control. 2021 June ; 68(6): 2075–2085. doi:10.1109/TUFFC.2021.3055498.

Simultaneous Noise Suppression and Incoherent Artifact Reduction in Ultrafast Ultrasound Vascular Imaging

Chengwu Huang[1], **Pengfei Song**[1,3,4], **Joshua D. Trzasko**[1], **Ping Gong**[1], **U-Wai Lok**[1], **Shanshan Tang**[1], **Armando Manduca**[2], **Shigao Chen**[1]

[1]Department of Radiology, Mayo Clinic College of Medicine and Science, Rochester, MN 55905, USA

[2]Department of Physiology and Biomedical Engineering, Mayo Clinic College of Medicine and Science, Rochester, MN 55905 USA

[3]Department of Electrical and Computer Engineering, University of Illinois at Urbana-Champaign, Urbana, IL, 61801

[4]Beckman Institute for Advanced Science and Technology, University of Illinois at Urbana-Champaign, Urbana, IL, 61801

Abstract

Ultrasound vascular imaging based on ultrafast plane wave imaging and singular value decomposition (SVD) clutter filtering has demonstrated superior sensitivity in blood flow detection. However, ultrafast ultrasound vascular imaging is susceptible to electronic noise due to the weak penetration of unfocused waves, leading to a lower signal-to-noise ratio (SNR) at larger depths. In addition, incoherent clutter artifacts originating from strong and moving tissue scatterers that cannot be completely removed create a strong mask on top of the blood signal that obscures the vessels. Herein, a method that can simultaneously suppress the background noise and incoherent artifacts is proposed. The method divides the tilted plane or diverging waves into two sub-groups. Coherent spatial compounding is performed within each sub-group, resulting in two compounded datasets. An SVD-based clutter filter is applied to each dataset, followed by a correlation between the two datasets to produce a vascular image. Uncorrelated noise and incoherent artifacts can be effectively suppressed with the correlation process, while the coherent blood signal can be preserved. The method was evaluated in wire-target simulations and phantom, in which around 7 dB to 10 dB SNR improvement was shown. Consistent results were found in a flow channel phantom with improved SNR by the proposed method (39.9 ± 0.2 dB) against conventional power Doppler (29.1 ± 0.6 dB). Last, we demonstrated the effectiveness of the method combined with block-wise SVD clutter filtering in a human liver, breast tumor and inflammatory bowel disease datasets. The improved blood flow visualization may facilitate more reliable small vessel imaging for a wide range of clinical applications, such as cancer and inflammatory diseases.

Corresponding Author: Shigao Chen (Chen.Shigao@mayo.edu).

Keywords

Ultrasound small vessel imaging; singular value decomposition (SVD); ultrafast ultrasound; noise suppression; artifact suppression

I Introduction

Microvasculature detection and quantification are critical for the evaluation of many physiological states, and pathological diseases such as cancer, chronic kidney diseases, and inflammatory diseases. Ultrasound imaging is a safe, widely available, and cost-effective modality that has been used in clinical practice for decades to detect and evaluate blood flow *in vivo*. Recently, the ultrasound small vessel imaging technique based on high frame-rate ultrasound imaging (i.e., plane wave imaging) and advanced tissue clutter filters (e.g., eigen-based filters, SVD-based filters) has demonstrated superior Doppler sensitivity to slow flow in small vessels without the need for an injection of ultrasound contrast microbubbles. The technique enables the detection of vasculature that may otherwise be invisible to conventional Doppler ultrasound [1-9].

One significant drawback of plane wave imaging-based small vessel imaging, however, is the low signal-to-noise ratio (SNR) due to the weak penetration of unfocused waves in the deep tissue region. To compensate for the weaker blood flow signal in deeper tissue regions due to ultrasound attenuation, we typically apply a depth-dependent time-gain compensation (TGC) to received signals, which will subsequently elevate the electronic noise floor at larger depths [10-12]. Owing to both the depth-dependent TGC and beamforming processes, this background electronic noise can be spatially varying, resulting in a spatially-dependent noise floor added to the ultrafast vascular images. Small vessel signals can be severely contaminated by the background noise in the deep region of the image [10, 11].

There have been many methods proposed to tackle this low SNR issue. For instance, noise is typically related to the high-order singular values and can be partially suppressed by removing the high-order singular values in SVD-based filtering [4, 12, 13]. By leveraging the spatial coherence of the blood signal, Dahl *et al* [14] and Li *et al* [15, 16] developed a coherent flow power Doppler (CFPD) technique that has demonstrated superior flow detection, uncorrelated noise and reverberation suppression over conventional power Doppler (PD) imaging. The real-time capability of CFPD was also demonstrated in a recent study [17]. Ozgun *et al* [18] provided a modification to CFPD by calculating the non-normalized coherence metric that preserved a linear relationship between image intensity and magnitude of the blood echo. Stanziola *et al* and Leow *et al* [19, 20] proposed an acoustic sub-aperture processing (ASAP) technique based on splitting the ultrasound channel data into two non-overlapping subgroups that lead to two subsets of images after beamforming. Correlation of these two subsets of images provided effective suppression of noise and improvement of the image contrast, given that noise is uncorrelated between channels. Tremblay-Darveau *et al* [21] demonstrated the improvement of PD imaging in terms of noise floor suppression, by using higher lags instead of the zero-lag of the autocorrelation, given that noise is completely uncorrelated from pulse-to-pulse. Bar-Zion *et*

al [22] exploited the temporal fluctuation characteristic of the contrast-enhanced ultrasound (CEUS) signal by calculating the high order signal statistics to achieve both resolution enhancement and background noise suppression.

Another significant challenge in ultrafast vascular techniques involves the incoherent clutter artifacts (such as side lobe and grating lobe artifacts) that result from the hyperechoic moving tissue scatters. The residual clutters of these strong-reflecting and moving tissue scatters after SVD clutter filtering can generate a strong mask superimposed on the blood signal, which obscures the visualization and quantification of the vasculature. These kinds of artifacts are more commonly observed *in vivo* via ultrafast Doppler imaging when tissue motion is pervasive and tissue scattering is typically strong and heterogeneous. These side lobes of the moving tissue scatters can be difficult to remove completely, which significantly hinders the *in vivo* performance of small vessel imaging. We have previously proposed several methods for background noise suppression and equalization [4, 10, 11]. However, an effective method targeting these incoherent clutter artifact suppression is still limited. Therefore, in this study, we present a method that can address this issue by simultaneously suppressing noise bias and incoherent clutter artifacts via correlation of blood flow signals generated from various beam steering angles.

II Methods

A. Simultaneous noise and artifact suppression

Assuming the clutter filtered signal (S) consists of complex blood flow signal and additive noises:

$$S(x,z,t) = B(x,z,t) + n(x,z,t) \tag{1}$$

where B is complex blood signal, n is the additive noise, x and z correspond to the lateral and axial dimensions of the ultrasound image, respectively, and t corresponds to the temporal dimension (referred to the slow-time dimension). The PD image can be calculated as the power of the Doppler signal at each spatial pixel, and the expectation of a PD image is given by:

$$\begin{aligned} E[PD(x,z)] &= E[\sum_{t=1}^{N_t} S(x,z,t)S^*(x,z,t)] \\ &= E[\sum_{t=1}^{N_t} \mid B(x,z,t) \mid^2] + E[\sum_{t=1}^{N_t} \mid n(x,z,t) \mid^2] \end{aligned} \tag{2}$$

where the cross-terms have zero expectation (since blood signal and noise are uncorrelated) and have been removed. Here * indicates complex conjugate, and N_t is the ensemble size. Therefore, the spatially-varying noise power ($\Sigma|n(x, z, t)|^2$) can be considered as an additive bias added to the PD image of the pure blood signal ($\Sigma|B(x, z, t)|^2$), which leads to the typical ramp-shaped background noise in ultrafast small vessel images.

The proposed method is based on the framework of ultrafast ultrasound compounding imaging, where multiple plane waves (or diverging waves for curved array) are typically

transmitted sequentially with different steering angles and the received signals are coherently added to generate a compounded ultrasound image [5, 23]. The schematic diagram of the proposed method is depicted in Fig. 1. Instead of a coherent sum on all the angles for compounding, the proposed method divides the tilted plane wave or diverging wave transmissions into two groups, followed by compounding within each group to generate two compounded data sets. For example, for 16-angle spatial compounding imaging, angles 1-8 can be treated as group 1, and angles 9-16 can be treated as group 2. The SVD-based clutter filtering will then be applied to each data set to remove tissue clutters [2, 4, 10], and the remaining data matrix for each group can be expressed as in Eqn. 1. For simplicity, the incoherent clutter artifacts and other non-additive noise are not included in Eqn. 1. The ultrasound vascular image is generated by calculating the correlation of the two clutter-filtered data sets, as:

$$\begin{aligned} UVI(x,z) &= \sum_{t=1}^{N_t} S_1(x,z,t)S_2^*(x,z,t) \\ &= \sum_{t=1}^{N_t} B_1(x,z,t)B_2^*(x,z,t) + \sum_{t=1}^{N_t} n_1(x,z,t)n_2^*(x,z,t) \\ &\quad + \sum_{t=1}^{N_t} B_1(x,z,t)n_2^*(x,z,t) + \sum_{t=1}^{N_t} B_2^*(x,z,t)n_1(x,z,t) \end{aligned} \tag{3}$$

where S_1, S_2 are the filtered signals from the two separated data sets, containing blood flow signal blood signal B_1, B_2 and additive noise n_1 and n_2, respectively. Since noise n_1 and n_2 are independent and uncorrelated, and are also uncorrelated with the blood signals B_1 and B_2, the cross-terms and the noise correlation term all have zero expectation, *i.e.* $E[\Sigma B_1(x, z, t)n_2{*}(x, z, t) + \Sigma B_2{*}(x, z, t)n_1(x, z, t)] = 0$ and $E[\Sigma n_1(x, z, t)n_2{*}(x, z, t)] = 0$. Given the ultrafast imaging PRF, the blood flow signals from the two data sets B_1, B_2 are assumed to be significantly coherent. Therefore, the expected ultrasound vascular image can be given by:

$$E[UVI(x,z)] = E[\sum_{t=1}^{N_t} B_1(x,z,t)B_2^*(x,z,t)] \tag{4}$$

where terms associated with noise interference are eliminated, coherent blood flow signal is preserved, which resembles the PD image of the pure blood signal.

The spatially incoherent clutter artifacts originating from the hyperechoic tissue are angle-dependent: the orientation of the “butterfly-shaped” side lobe and grating lobe vary with the transmitting angle. Therefore, the artifacts from the same scattering source in the two distinct compounded data sets should be spatially incoherent or partially incoherent, considering the angle difference of the transmission. The calculation of the correlation of these two data sets (Eq. 3) would thus suppress these spatially incoherent components while enhancing the coherent blood flow signal.

In addition to correlation with zero-lag in the temporal direction, the proposed method can be extended to an arbitrary temporal lag:

$$UVI(x,z,k)=\sum_{t=1}^{N_t-k} S_1(x,z,t+k)S_2^*(x,z,t) \tag{5}$$

where k is the lag in frames (k is an integer). A smaller k or a higher frame rate would be preferred to maintain the blood signal coherence. The vascular images obtained with different k values can be combined via a weighted sum to further improve noise suppression and enhance image contrast:

$$UVI(x,z)=\sum_{k} UVI(x,z,k)w(x,z,k) \tag{6}$$

where $w(x, z, k)$ is the weight and can be determined based on the coherence of the blood signal or can be equal for all k values for an averaging calculation. For simplicity, in this study the vascular image was generated by summing correlations with $k = 0$ and $k = 1$ (i.e., $w(x, z, k) = 1$). Since IQ data was used for SVD clutter filtering, a complex UVI image would be produced according to the above equations. Therefore, in this study, the absolute value of the complex image was used as the final vascular image. The conventional PD image was generated by zero-lag correlation, as indicated by Eqn. (2). In this study, either PD images, or proposed vascular images are displayed in a logarithmic scale (i.e., $10\log_{10}()$) for visualization.

B. Implementation to block-wise adaptive SVD filtering

The block-wise adaptive SVD filtering was previously proposed to facilitate robust and simultaneous tissue clutter and noise rejection [4]. Given the complex spatial distribution of tissue clutter and noise *in vivo,* especially for in human imaging with large FOV, local block-wise SVD filtering was shown to achieve a much improved clutter rejection and blood signal extraction based on local data statistics than a global SVD filtering that was solely based on the global data characteristic. In the original block-wise SVD, the ultrasound data were decomposed into spatially overlapping small blocks. And SVD was calculated for each block to reject tissue clutter and noise, by removing low-order singular values related to tissue clutters and high-order singular values corresponding to noise [4]. Normalization to the remaining signal energy after tissue clutter and noise rejection in each block was applied in this technique, which facilitated equalizing the uneven noise distribution and improved visualization of small vessels. However, incoherent clutter artifacts could not be removed in this process and may be enhanced by the local power normalization similar to that of the real blood flow signal. Here we propose to incorporate the correlation method into block-wise SVD filtering to enable incoherent artifact suppression while leveraging the advantages of the block-wise SVD filter (e.g., locally and adaptively adjusted singular value cutoff and redundant combinations of overlapped blocks for enhanced performance). The same signal processing step as described in section A was implemented for each block of data. Specifically, assume that an original subset of data $\boldsymbol{S}_{0i}$ for block i had a dimension of $x_i \times z_i \times t_i$ (x_i, z_i and t_i correspond to lateral, axial, temporal dimensions, respectively). $\boldsymbol{S}_{0i}$ was first reshaped as a Casorati matrix $\boldsymbol{C}_{0i}$ with a dimension of $x_i z_i \times t_i$, in which the columns were the vectorized frames, followed by a calculation of SVD, as $\boldsymbol{C_{0i}} = \boldsymbol{U}_{0i}\boldsymbol{D}_{0i}\boldsymbol{V}_{0i}^T$, where $\boldsymbol{U}_{0i}$ and $\boldsymbol{V}_{0i}$

were orthonormal matrices whose columns were the left and right singular vectors of $\boldsymbol{C}_{0i}$, respectively, and $\boldsymbol{D}_{0i}$ was the diagonal matrix whose diagonal entries are the singular values, expressed as $D_{0i} = \mathrm{diag}(\sigma_{i1}, \sigma_{i2}, \cdots, \sigma_{iN_t})$, with singular values sorted in descending order [2, 4]. The number of lower-order singular values (e.g., l_i) related to the tissue clutter to be removed was adaptively determined by the decay rate of the singular value curve [4], and the filtered matrix was obtained by: $\widehat{C}_{0i} = U_{0i}\widehat{D}_{0i}\boldsymbol{V}_{0i}^{T}$, where $\widehat{D}_{0i}$ was the diagonal matrix with the first l^{th} singular values removed, $\widehat{D}_{0i} = \mathrm{diag}(0, \cdots, 0, \sigma_{i(l_i+1)}, \sigma_{i(l_i+2)}, \cdots, \sigma_{iN_t})$. The filtered Casorati matrix can then be reshaped back to the original dimension to obtain the clutter filtered signal $\boldsymbol{S}_i$. This SVD process was implemented on the two subsets of data for each block, resulting in the two SVD-filtered signals $\boldsymbol{S}_{1i}$ and $\boldsymbol{S}_{2i}$. The vascular image for this block $UVI_{Block,i}$ was generated by the correlation of $\boldsymbol{S}_{1i}$ and $\boldsymbol{S}_{2i}$ according to the Eqn. 5 and 6. Since uncorrelated noise can be suppressed by the correlation of the two subsets of data for each local block, removal of the high-order singular values that is used in the original block-wise SVD filtering is not necessary. For each block, normalization of $UVI_{Block,i}$ to the geometric mean of the signal energy of the two correlating data $\boldsymbol{S}_{1i}$ and $\boldsymbol{S}_{2i}$ (equals to $\sqrt{(\sum_{j=l_{1i}+1}^{N_t}\sigma_{1i,j}^2)\cdot(\sum_{j=l_{2i}+1}^{N_t}\sigma_{2i,j}^2)}$, where $\sigma_{1i,j}$ and $\sigma_{2i,j}$ are the singular values for the two subsets for the block i, and l_{1i} and l_{2i} are the corresponding number of lower-order singular values to be removed) was applied, before combining all the images of the small blocks to generate the full FOV vascular image, as[4]:

$$UVI_{LocalSVD}(x,z) = \frac{1}{M}\sum_{i=1}^{M}\frac{UVI_{Block,i}(x,z)}{\sqrt{(\sum_{j=l_{1i}+1}^{N_t}\sigma_{1i,j}^2)\cdot(\sum_{j=l_{2i}+1}^{N_t}\sigma_{2i,j}^2)}} \quad (7)$$

where M is the total number of overlapped blocks containing the pixel (x, z). In the case where a block contains noise only, the vascular image of this block $UVI_{Block,i}$ will have zero expectation according to Eqn. 4, and will be normalized to the geometric mean of the noise energy of the two subsets in the given block.

C. Simulation, phantom experiments, and in vivo validation

To evaluate the effect of the proposed method on the point-spread-function (PSF), we simulated a series of wire targets at different depths using the embedded Verasonics Research Ultrasound Simulator on a Verasonics Vantage ultrasound system (Verasonics Inc., Kirkland, WA, USA). The same imaging setups were used for simulation, phantom and *in vivo* imaging using a GE 9L linear array transducer (GE Healthcare, Wauwatosa, WI). The detailed imaging setups were summarized in Table I. The same ultrasound system and transducer (GE 9L) was used to acquire data of wire targets from a CIRS standard tissue phantom (Model 040GSE, CIRS, Norfolk, VA, USA). Free-hand scanning was used for data acquisition in order to introduce tissue motion during data acquisition to enhance the clutter artifacts from the strong scattering wire targets, which emulates the artifacts observed *in vivo*. The same ultrasound system was also used to acquire ultrasound data from a horizontal flow channel in an ultrasound Doppler phantom (Model 1425, Gammex, Middleton, WI, USA) for validation of the proposed vascular imaging in both background noise and artifact suppression. The image view was carefully adjusted to include a section of the flow channel

and the wire targets. For the phantom experiments, a 16-angle plane wave transmission was implemented, as detailed in Table I.

For *in vivo* validation, *in vivo* data sets were acquired from a healthy human liver, a human breast tumor, and a terminal ileum (TI) segment of human bowel with Crohn's disease. All of the data were acquired with free-hand scanning with the purpose of inducing incoherent artifacts in the vascular image (supplemental videos show the artifacts can be more easily generated with tissue motions). The same transducer (GE 9L-D) and imaging settings were used for breast tumor data acquisition, while the liver data were acquired with a GE C1-6-D (GE Healthcare, Wauwatosa, WI) curved array transducer (see Table I for detailed imaging setups). In-phase/quadrature (IQ) data were saved for post-processing. The imaging angles were equally separated into two subgroups for small vessel imaging (e.g., angles 1-8 as group 1, angles 9-16 as group 2 for the 16-angle transmission). All the *in vivo* human studies were approved by the Institutional Review Board of Mayo Clinic.

III Results

The simulated wire targets at different depths are shown in Fig. 2. Analogue to the blood flow image, the wire targets are also displayed as the PD or signal correlation via the proposed method. Fig. 2a is the PD image of the data obtained from the compounding of all angle transmissions. A relatively high dynamic range was utilized here to visualize both the side lobes and grating lobes in the images. With tilted plane wave data split into two subgroups (Fig. 1) and compounded separately, two sets of ultrasound data were obtained, and their PD images are shown in Fig. 2b. The correlation of the two sets of ultrasound data resulted in the final wire targets image, as shown in Fig. 2c, where spatially incoherent side-lobe or grating lobe components can be partially suppressed compared to Fig. 2a. Figs. 2d and 2e are the zoom-in region of the wire target indicated by the white rectangle in Figs. 2a and 2c, respectively. Those side lobe components that are not spatially overlapped in Fig. 2b can be suppressed, as denoted by the white arrows in Fig. 2d. Fig. 2f quantitatively depicts lateral profiles of a wire target at around 40 mm depth from the PD image (Fig. 2a) and the proposed vascular image (Fig. 2c), showing around a 10 dB improvement at the grating lobe region of the image. Axial profiles of the grating lobes of the wire targets at a lateral position of around 20 mm (indicated by the vertical line in Fig. 2a) are shown in Fig. 2g, revealing an overall suppression of grating lobes by the proposed method. A ~18 dB improvement was shown at a depth of around 35 mm in the axial profile via the proposed correlation-based method.

To mimic a more realistic situation, wire targets were imaged from a tissue phantom (B-mode image shown in Fig. 3a) using free-hand scanning with small probe motion. Similar to blood flow imaging, a full SVD-clutter filtering was applied to remove tissue clutters, and the resulting PD image is shown in Fig. 3b. The residual clutters originated from strong-reflecting wire targets or scatters shown in Fig. 3b represent the artifacts that appear in the small vessel images undermining the visualization of the vasculature. With the proposed method, the contrast of the image can be improved by the suppression of those spatially incoherent artifacts, as shown in Fig. 3c. Figures 3d and 3e depict a horizontal profile and

vertical profile along the white lines denoted in Fig. 3b, showing an average improvement of a contrast of 7.0 dB and 9.3 dB along the horizontal profile and vertical profile, respectively.

For flow channel phantom imaging, the original PD images filtered by the full SVD clutter filter on the full-angle compounded data are shown in Fig. 4a, where the background noise bias and the side lobe artifacts generated from the hyperechoic wire targets are clearly present. By using the proposed method, both the noise bias and the side-lobe artifacts can be suppressed, providing higher contrast and better visualization of the blood flow image, as shown in Fig. 5a. For quantitative evaluation, SNR of the vascular image is defined as the ratio of the mean value of the blood flow region and the background region. Here the blood flow ROI is selected inside the flow channel, as indicated by the black rectangle in Fig. 5a. Four background ROIs are selected at the same depth, each providing an SNR measurement, and the final SNR estimate is shown as the mean SNR ± standard deviation of the four estimates. The SNR estimates were calculated on the original PD image and the final vascular images generated by summing correlations with $k = 0$ and $k = 1$ based on Eqn. 6. The quantitative SNR of the vascular image obtained with the proposed method is 39.9 ± 0.2 dB (Fig. 5a), which is substantially improved compared to that of the original PD image (Fig. 4a, 29.1 ± 0.6 dB). The side lobe artifacts are largely suppressed (as shown in Fig. 5a), indicating the effectiveness of the proposed method.

The original PD image of the human liver processed with full SVD filtering is shown in Fig. 4b, where the small vessels can be overshadowed by the background noise bias, especially for mid-to-deep imaging regions. However, the noise bias and the incoherent clutter artifacts (indicated by the arrows in Fig. 4b) can again be partially suppressed with the proposed method (Fig. 5b), enabling a much better visualization of the liver vasculature with substantially improved contrast. Quantitative SNR was also estimated from a selected vascular ROI (indicated by the black rectangle in Fig. 5b) and a background ROI (denoted by the white rectangle in Fig. 5b). The SNR obtained by the proposed vascular imaging is 26.7 dB, which is about 8.2 dB higher than that of the PD image (18.5 dB, Fig. 4b) estimated from the same ROIs.

The vascular image of the same liver data obtained with the block-wise SVD filtering is shown in Fig. 6. Figure 6a is the liver vascular image obtained with the original block-wise SVD filtering, where the noise was suppressed by rejecting the high-order singular values [4]. However, the side lobe artifacts from the hyperechoic tissue scatterers remained and were even enhanced by block-wise SVD processing. By incorporating the proposed method into block-wise SVD, as shown in Fig. 6b, both background noise and side lobe artifacts were removed. One can see the benefit of performing block-wise SVD in the mid-upper region of the liver, where tiny vessels that are invisible in conventional block-wise SVD and global SVD become clearly visible.

The vascular images of the breast tumor and human bowel segment obtained with block-wise local SVD filtering are shown in Fig. 7, where Fig. 7a and 7b are the original vascular images without artifact suppression, and Fig. 7c and 7d are the corresponding vascular images with the proposed method. Again for the *in vivo* application, the vasculature can be strongly overwhelmed by the side lobe artifacts, which severely deteriorate the visualization

of the vessel structure, as indicated in Fig. 7a and 7b. The proposed method, however, can largely suppress those strong artifacts in block-wise SVD processing, and improve small vessel detection, as shown in Fig. 7c and 7d. With suppression of artifacts, subsequent quantification of the vasculature, such as vessel density, can be obtained more accurately. Taking the breast tumor as an example, one can easily apply a threshold (−16 dB was used here) to Fig. 7c to obtain a binary image for area calculation (Fig. 8b) that better represents the true vessel density than that without artifact suppression (Fig. 8a). The presence of strong artifacts in Fig. 7a typically results in an overestimation of the vessel area, and leads to a biased vessel density estimation.

IV Discussion

A method for suppression of background noise bias and incoherent clutter artifacts in ultrafast ultrasound vascular imaging was proposed in this study. The substantial improvement of the ultrafast vascular image that can be achieved in simulation, phantoms, and *in vivo* data demonstrated the effectiveness of the proposed method, especially for *in vivo* applications where the incoherent clutter artifacts can be significant (e.g., Fig. 7). The simultaneous suppression of noise bias and incoherent clutter artifacts may facilitate a more accurate interpretation of disease based on state-of-the-art high sensitive ultrafast vascular imaging.

The proposed method takes advantage of the uncorrelated nature of noise and the incoherence of clutter artifacts in ultrasound data of different steering angles. In this study, the number of transmitting angles was equally divided into two groups. However, the number of angles in each subgroup can potentially be arbitrary. The noise can be effectively suppressed as long as they are random and uncorrelated between subgroups. However, dividing the total angle number in half will lead to SNR drops in each subgroup. To increase the SNR and resolution of the final vascular image, a larger number of transmitted angles will be preferable, but at the cost of the compounded frame rate of the ultrasound imaging [24]. Except for background noise, another consideration is the coherence of the side lobe or grating lobe artifacts in the two subgroups of data. Given that the PSF or the orientation of the side lobe and grating lobe are transmitting angle-dependent (Fig. 2b), a larger angle span between subgroups will increase the incoherence of these artifacts [25]. Therefore, maximizing the transmitting angle difference between subgroups may be optimal for side lobe and grating lobe artifact suppression in vascular imaging. However, according to the angular coherence theory, increasing the transmitted angle span will decrease the coherence of the targeted blood flow signal, potentially deteriorating the correlation-based vascular image [26]. Furthermore, transducer element directivity will also need to be considered, which limits the maximum transmitted angle. Overall, a tradeoff exists between the performance of artifact suppression and blood signal coherence. Another factor that is related to the decorrelation of the blood signal is the blood flow speed: a faster flow tends to have lower signal coherence between subgroups. In this case, a higher frame rate or PRF will be preferred to minimize the decorrelations brought by blood flow, especially for fast flow in big vessels.

This study focused on suppressing the background noise bias and uncorrelated clutter artifacts in ultrafast vascular imaging to improve the visualization of small vessels. However, subsequent quantification indices, such as vascular density and morphological indices, based upon the improved small vessel image may also be derived potentially with higher accuracy or consistency for disease evaluation and monitoring [27, 28]. For instance, vessel density is a typical index for accessing tissue vascularity by estimating the percentage area or volume of the vessel. Vessel area or volume can typically be calculated as the area or volume of the vascular image with intensity above a selected threshold. The strong artifacts will lead to difficulties in separating artifacts from true blood signals, typically resulting in an overestimation of the vessel area, and thus biasing the estimation of vessel density. Similarly, quantitative indices like curvature, tortuosity, vessel size, or vessel number, can potentially be obtained more accurately with the suppression of these artifacts and background noise. Original ultrasound power Doppler images represent the backscattering power of the moving blood cells, and reflect the blood volume at vessel locations [29]. The proposed method provides a better image that also represents the backscattering signal power of the moving blood by multiplication of signals of the same blood volume from two steering angles, which may better represent the blood volume with the suppression of the background noise and artifacts. However, given that there is a small time-delay between ultrasound transmissions for the two subsets of data, the vascular intensity in the proposed image may be underestimated due to the decorrelation of the blood flow signal for the fast flow, and may thus result in underestimation of blood volume in larger vessels.

In this study, the proposed method was first evaluated using a global SVD filtering, where the capability of simultaneous suppression of background noise and incoherent artifacts was shown. The method was then implemented in block-wise adaptive SVD filtering, which has better performance in the separation of tissue clutter and blood flow signal based on local data statistics [4]. It should be noted that quantitative SNR was only calculated in the global SVD filtering (Fig. 4 and 5) to compare the performance before and after applying the correlation-based method. In block-wise SVD filtering, the local blood signal and noise are normalized to their energies, which had unevenly changed the signal and noise levels in different regions. Thus the calculation of SNR by comparing blood signal in one ROI to noise in another ROI will be biased and not included in the block-wise SVD filtering in this study. In the original block-wise SVD filtering, noise can be suppressed by removing high-order singular values, which will potentially reject portions of blood flow signals. Using the proposed method, uncorrelated noise can be suppressed without the need to reject higher-order singular values, which may contribute to better small vessel detection, as shown in Fig. 6b compared with Fig. 6a, especially in the upper and middle regions of the liver. Normalization to local signal energy in each block was used in the block-wise SVD filtering to improve the appearance of small vessels, which may also lead to the slight discrepancy of local signal intensity observed in Figs. 6a, and 6b. In Fig. 6b, there is a slightly enhanced tissue clutter in the near field compared with Fig. 6a, and Fig. 5b, which is probably because of the normalization to the remaining energy after SVD filtering for each individual local block of data, according to Eqn. 7, which has the potential to bring up weak clutter signals in the blocks without blood signals.

The simulation experiment (Fig. 2) showed that the lateral resolution of wire-targets decreased by the proposed method, which is expected because only half the transmitting angles were used for each subset. However, this finding is opposite to realistic situations shown in tissue phantom imaging (Fig.3) and in-human tissue imaging (Fig. 7), where the lateral resolution was visually improved by the proposed method. One possible explanation is that the lateral resolution of the vessel image seems to have deteriorated in the complicated situation *in vivo* with the presence of strong artifacts and noise. Suppression of these uncoherent artifacts and noise produces the impression of improved resolution, even though the main lobe becomes slightly broader. In the block-wise SVD clutter filtering without using the correlation method (Fig. 7), energy normalization that enhances small vessel signals may also enhance the artifacts that deteriorate small vessel identification. Instead, combined with the proposed method, these artifacts were first suppressed before energy normalization, and thus, the small vessels were better enhanced with a cleaner and sharper visualization (Fig. 7). One limitation of the proposed method is that since the ultrasound data are split into two subsets, SVD-based clutter filtering needs to be performed twice, which doubles the computational cost for the ultrafast vascular imaging. We previously proposed an accelerated SVD-based filtering technique that can substantially improve the computational efficacy and can be potentially implemented in real-time when combined with parallel processing [30, 31], which may alleviate the computational burden of the proposed method. Furthermore, the proposed method can be applied to other tissue clutter filtering methods, such as high-pass temporal filtering, where the computational cost would no longer be a major obstacle. There are also other methods that leverage the concept of signal coherence to suppress noise based on tissue clutter filtering in the context of either non-contrast or contrast-enhanced ultrasound imaging as summarized in the introduction [13, 15, 16, 18-22]. Among these methods, ASAP split the channel data for each transmitted angle before beamforming and achieved effective noise suppression by calculating the correlation between split data [19, 20]. The proposed method in this study, however, split the transmitting angle beamformed data before spatial compounding for correlation. Except for background noise floor suppression, the proposed method targets effective artifact suppression by leveraging the transmitted angle-dependent incoherence of the side lobe and grating lobe in vascular imaging. While our method was demonstrated for contrast-free vascular imaging, the principle may also be readily applied to contrast-enhanced ultrasound imaging for noise and artifact suppression.

V Conclusion

A method that can simultaneously suppress the noise-induced bias and incoherent clutter artifacts (such as side lobe and grating lobe artifacts) in the ultrafast ultrasound vascular image was proposed. The feasibility and effectiveness of the method were demonstrated with simulation, phantom and *in vivo* experiments, showing marked improvement of small vessel image for vasculature visualization. The proposed method has great potential to facilitate better implementation of ultrafast ultrasound vascular imaging into a wide range of clinical applications such as cancer and inflammatory disease evaluation.

The study was supported in part by the National Cancer Institute of the National Institutes of Health under Award Number R00CA214523 and National Institute of Diabetes and

Digestive and Kidney Diseases under Award Number R01DK120559. The content is solely the responsibility of the authors and does not necessarily represent the official views of the National Institutes of Health. The authors would like to thank Ms. Jennifer L. Poston for her assistance in editing the manuscript.

Supplementary Material

Refer to Web version on PubMed Central for supplementary material.

References

[1]. Bercoff J et al., "Ultrafast Compound Doppler Imaging: Providing Full Blood Flow Characterization," IEEE Trans. Ultrason. Ferroelectr. Freq. Control, vol. 58, no. 1, pp. 134–147, 1 2011. [PubMed: 21244981]

[2]. Demene C et al., "Spatiotemporal Clutter Filtering of Ultrafast Ultrasound Data Highly Increases Doppler and fUltrasound Sensitivity," IEEE Trans. Med. Imaging, vol. 34, no. 11, pp. 2271–2285, 11 2015. [PubMed: 25955583]

[3]. Mace E, Montaldo G, Cohen I, Baulac M, Fink M, and Tanter M, "Functional ultrasound imaging of the brain," Nat. Methods, vol. 8, no. 8, pp. 662–U85, 8 2011. [PubMed: 21725300]

[4]. Song PF, Manduca A, Trzasko JD, and Chen SG, "Ultrasound Small Vessel Imaging With Block-Wise Adaptive Local Clutter Filtering," IEEE Trans. Med. Imaging, vol. 36, no. 1, pp. 251–262, 1 2017. [PubMed: 27608455]

[5]. Tanter M and Fink M, "Ultrafast Imaging in Biomedical Ultrasound," IEEE Trans. Ultrason. Ferroelectr. Freq. Control, vol. 61, no. 1, pp. 102–119, 1 2014. [PubMed: 24402899]

[6]. Yu ACH and Lovstakken L, "Eigen-Based Clutter Filter Design for Ultrasound Color Flow Imaging: A Review," IEEE Trans. Ultrason. Ferroelectr. Freq. Control, vol. 57, no. 5, pp. 1096–1111, 5 2010. [PubMed: 20442020]

[7]. Kim M, Zhu Y, Hedhli J, Dobrucki LW, and Insana MF, "Multidimensional Clutter Filter Optimization for Ultrasonic Perfusion Imaging," IEEE Trans. Ultrason. Ferroelectr. Freq. Control, vol. 65, no. 11, pp. 2020–2029, 11 2018. [PubMed: 30183625]

[8]. Kang J, Go D, Song I, and Yoo Y, "Wide Field-of-View Ultrafast Curved Array Imaging Using Diverging Waves," IEEE Transactions on Biomedical Engineering, vol. 67, no. 6, pp. 1638–1649, 2020. [PubMed: 31562069]

[9]. Tierney J, Baker J, Brown D, Wilkes D, and Byram B, "Independent Component-Based Spatiotemporal Clutter Filtering for Slow Flow Ultrasound," IEEE Trans. Med. Imaging, vol. 39, no. 5, pp. 1472–1482, 2020. [PubMed: 31689187]

[10]. Song PF, Manduca A, Trzasko JD, and Chen SG, "Noise Equalization for Ultrafast Plane Wave Microvessel Imaging," IEEE Trans. Ultrason. Ferroelectr. Freq. Control, vol. 64, no. 11, pp. 1776–1781, 11 2017. [PubMed: 28880169]

[11]. Huang C, Song P, Gong P, Trzasko JD, Manduca A, and Chen S, "Debiasing-Based Noise Suppression for Ultrafast Ultrasound Microvessel Imaging," IEEE Transactions on Ultrasonics, Ferroelectrics, and Frequency Control, vol. 66, no. 8, pp. 1281–1291, 2019.

[12]. Nayak R, Fatemi M, and Alizad A, "Adaptive background noise bias suppression in contrast-free ultrasound microvascular imaging," Physics in Medicine & Biology, vol. 64, no. 24, p. 245015, 2019/12/19 2019. [PubMed: 31855574]

[13]. Baranger J, Arnal B, Perren F, Baud O, Tanter M, and Demene C, "Adaptive spatiotemporal SVD clutter filtering for Ultrafast Doppler Imaging using similarity of spatial singular vectors," IEEE Trans. Med. Imaging, vol. PP, no. 99, pp. 1–1, 2 2018.

[14]. Dahl JJ, Bottenus N, Bell MAL, and Cook MJ, "Coherent flow imaging: A power Doppler imaging technique based on backscatter spatial coherence," in 2013 IEEE International Ultrasonics Symposium (IUS), 2013, pp. 639–642.

[15]. Li YL and Dahl JJ, "Coherent Flow Power Doppler (CFPD): Flow Detection Using Spatial Coherence Beamforming," IEEE Trans. Ultrason. Ferroelectr. Freq. Control, vol. 62, no. 6, pp. 1022–1035, 6 2015. [PubMed: 26067037]

[16]. Li YL, Hyun D, Abou-Elkacem L, Willmann JK, and Dahl JJ, "Visualization of Small-Diameter Vessels by Reduction of Incoherent Reverberation With Coherent Flow Power Doppler," IEEE Trans. Ultrason. Ferroelectr. Freq. Control, vol. 63, no. 11, pp. 1878–1889, 11 2016. [PubMed: 27824565]

[17]. Li YL, Hyun D, Durot I, Willmann JK, and Dahl JJ, "High Sensitivity Liver Vasculature Visualization Using a Real-Time Coherent Flow Power Doppler (CFPD) Imaging System: A Pilot Clinical Study," in 2018 IEEE International Ultrasonics Symposium (IUS), 2018, pp. 1–9.

[18]. Ozgun K, Tierney J, and Byram B, "A Spatial Coherence Beamformer Design for Power Doppler Imaging," IEEE Trans. Med. Imaging, vol. 39, no. 5, pp. 1558–1570, 2020. [PubMed: 31725374]

[19]. Leow CH et al., "3-D Microvascular Imaging Using High Frame Rate Ultrasound and ASAP Without Contrast Agents: Development and Initial In Vivo Evaluation on Nontumor and Tumor Models," IEEE Transactions on Ultrasonics, Ferroelectrics, and Frequency Control, vol. 66, no. 5, pp. 939–948, 2019.

[20]. Stanziola A, Leow CH, Bazigou E, Weinberg PD, and Tang M-X, "ASAP: Super-Contrast Vasculature Imaging using Coherence Analysis and High Frame-Rate Contrast Enhanced Ultrasound," IEEE Trans. Med. Imaging, vol. PP, no. 99, pp. 1–1, 2 2018.

[21]. Tremblay-Darveau C et al., "Improved Contrast-Enhanced Power Doppler Using a Coherence-Based Estimator," IEEE Trans. Med. Imaging, vol. 36, no. 9, pp. 1901–1911, 9 2017. [PubMed: 28463190]

[22]. Bar-Zion A, Tremblay-Darveau C, Solomon O, Adam D, and Eldar YC, "Fast Vascular Ultrasound Imaging With Enhanced Spatial Resolution and Background Rejection," IEEE Trans. Med. Imaging, vol. 36, no. 1, pp. 169–180, 1 2017. [PubMed: 27541629]

[23]. Tanter M, Bercoff J, Sandrin L, and Fink M, "Ultrafast compound imaging for 2-D motion vector estimation: Application to transient elastography," IEEE Trans. Ultrason. Ferroelectr. Freq. Control, vol. 49, no. 10, pp. 1363–1374, 10 2002. [PubMed: 12403138]

[24]. Montaldo G, Tanter M, Bercoff J, Benech N, and Fink M, "Coherent Plane-Wave Compounding for Very High Frame Rate Ultrasonography and Transient Elastography," IEEE Trans. Ultrason. Ferroelectr. Freq. Control, vol. 56, no. 3, pp. 489–506, 3 2009. [PubMed: 19411209]

[25]. Denarie B et al., "Coherent Plane Wave Compounding for Very High Frame Rate Ultrasonography of Rapidly Moving Targets," IEEE Trans. Med. Imaging, vol. 32, no. 7, pp. 1265–1276, 7 2013. [PubMed: 23549887]

[26]. Li YL and Dahl JJ, "Angular coherence in ultrasound imaging: Theory and applications," J. Acoust. Soc. Am, vol. 141, no. 3, pp. 1582–1594, 3 2017. [PubMed: 28372139]

[27]. Demené C et al., "3-D Longitudinal Imaging of Tumor Angiogenesis in Mice in Vivo Using Ultrafast Doppler Tomography," Ultrasound in Medicine & Biology, vol. 45, no. 5, pp. 1284–1296, 2019/5/01/2019. [PubMed: 30799125]

[28]. Huang C et al., "Noninvasive Contrast-Free 3D Evaluation of Tumor Angiogenesis with Ultrasensitive Ultrasound Microvessel Imaging," Sci Rep, vol. 9, no. 1, p. 4907, 2019/3/20 2019. [PubMed: 30894634]

[29]. Rubin JM et al., "Fractional moving blood volume: estimation with power Doppler US," Radiology, vol. 197, no. 1, pp. 183–190, 1995. [PubMed: 7568820]

[30]. Song PF et al., "Accelerated Singular Value-Based Ultrasound Blood Flow Clutter Filtering With Randomized Singular Value Decomposition and Randomized Spatial Downsampling," IEEE Trans. Ultrason. Ferroelectr. Freq. Control, vol. 64, no. 4, pp. 706–716, 4 2017. [PubMed: 28186887]

[31]. Lok UW et al., "Real time SVD-based clutter filtering using randomized singular value decomposition and spatial downsampling for micro-vessel imaging on a Verasonics ultrasound system," Ultrasonics, vol. 107, p. 106163, 2020/9/01/2020. [PubMed: 32353739]

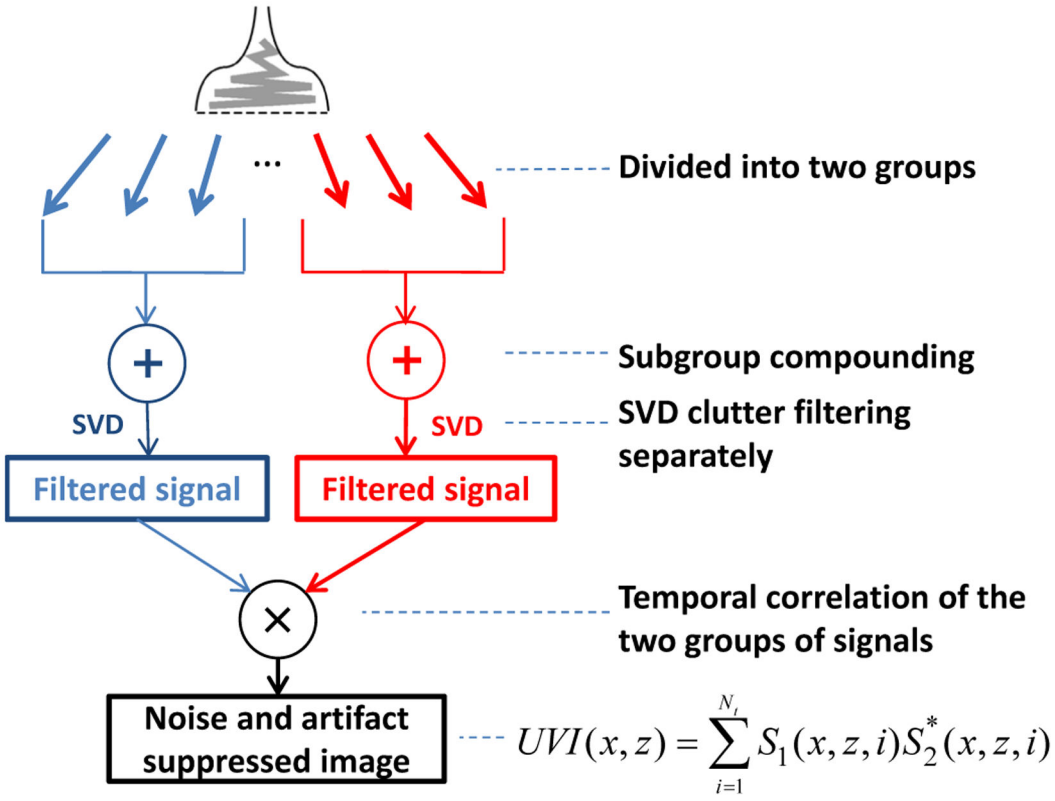

Fig. 1.
Schematic diagram of the proposed ultrafast ultrasound vascular imaging method

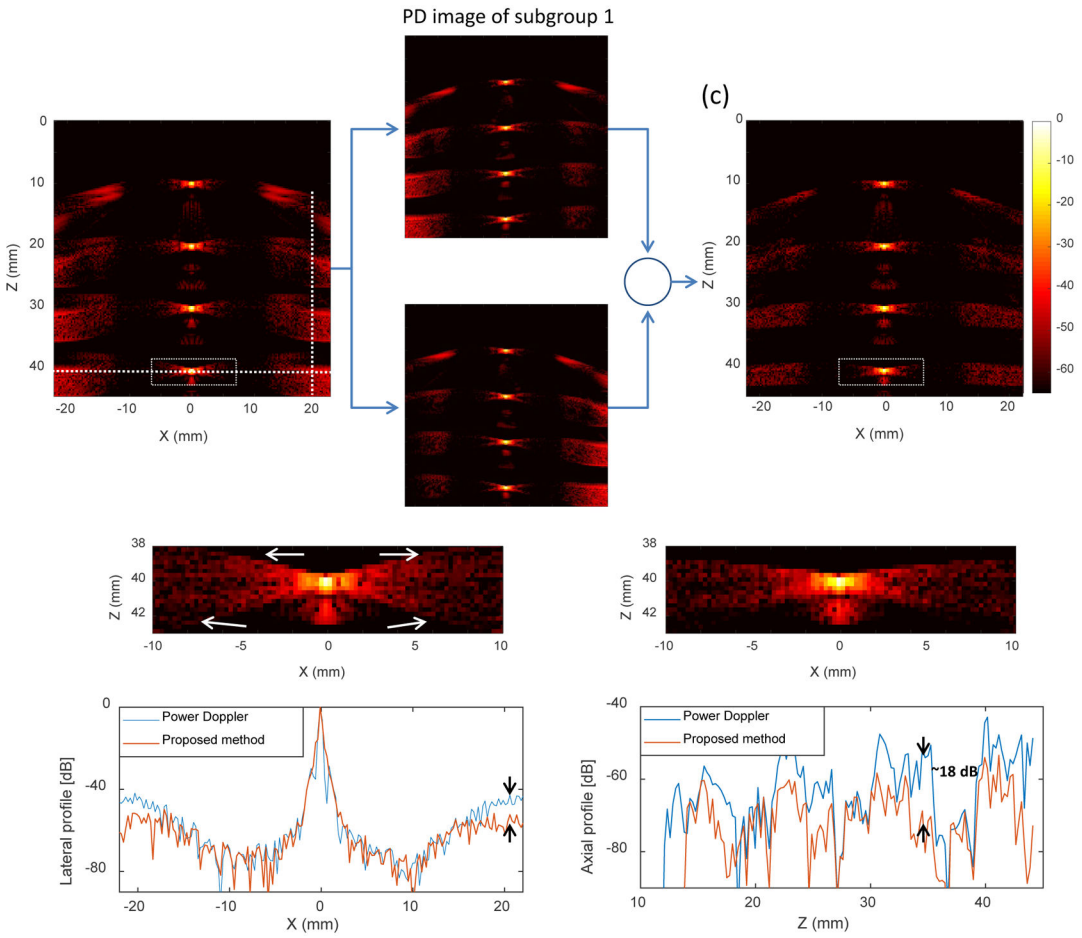

Fig. 2.

(a) Power Doppler (PD) image of the wire targets based on simulated all-angle compounding data. (b) PD images based on the simulated subgroup compounding data, revealing the angle-dependent side lobes and grating lobes of the wire targets. (c) The simulated wire target image using the proposed method based on the correlation of the subgroup compounding data. Fig. 2(a) to 3(c) are displayed as a $10*\log_{10}()$ scale with the same dynamic range of −65 dB to 0 dB. (d) and (e) are the zoom-in region of the wire target indicated by the white rectangle in (a) and (c), respectively. The spatially incoherent side lobe components indicated by the white arrows in (d) can be largely suppressed by the proposed method. (f) Lateral profile of the wire target at a depth of around 40 mm, indicated by the horizontal dashed line in (a). About 10 dB improvement of the profile at the lateral edge (grating lobes) was observed (indicated by the arrows). (g) Axial profile of the grating lobes at the lateral position of around 20 mm, indicated by the vertical dashed line in (a), showing an overall suppression of grating lobes (~18 dB improvement at the 35 mm depth, indicated by the arrows.

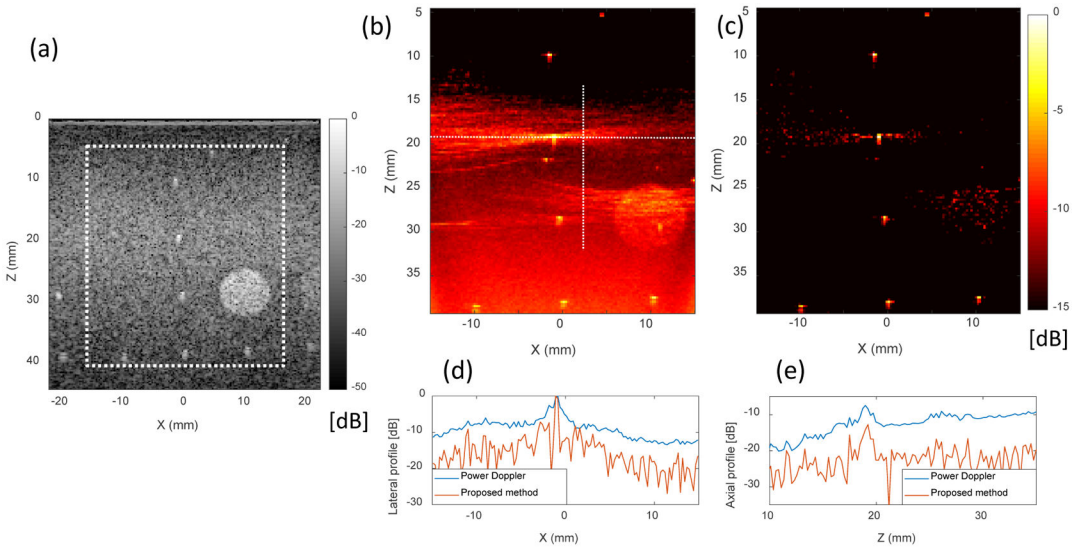

Fig. 3.

(a) B-mode image of the measured phantom. (b) Power Doppler (PD) image based on the all-angle compounding data of the phantom ROI indicated by the white rectangle in (a). PD image was generated from the clutter filtered data, and incoherent clutter artifacts original from the strong reflecting scatterers can be observed. (c) The proposed image obtained based on the correlation of the subgroup datasets, showing visualization improvement with clutter artifact suppression. Fig. 3(b) and 3(c) are displayed as a $10*\log_{10}()$ scale with the same dynamic range. (d) Lateral profile of the wire target at a depth of around 20 mm, indicated by the horizontal dashed line in (b), showing an average improvement of 7.0 dB of the profile obtained with the proposed method. (e) Axial profile along the vertical dashed line in (b), showing an average improvement of 9.3 dB of the profile using the proposed method.

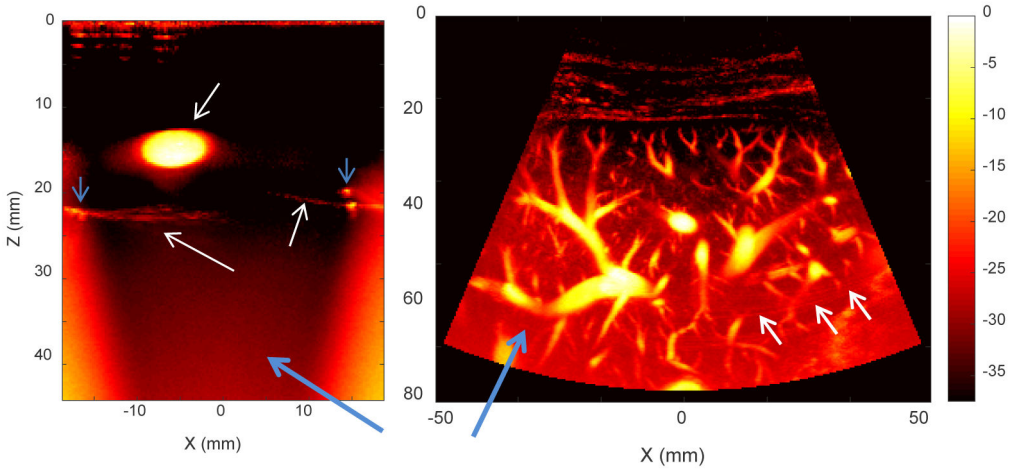

Fig.4.

(a) Blood flow phantom PD image obtained with full SVD clutter filtering. The side lobe of the wire targets (indicated by the blue arrows) cannot be completely removed by the clutter filtering and results in artifacts on the vascular image. (b) Human liver PD vascular image obtained with full SVD clutter filtering. The ‘ramp-shape’ noise bias and side lobe artifacts are present and indicated by the arrows. Both images are under the same color scale (−37.5 dB ~ 0 dB).

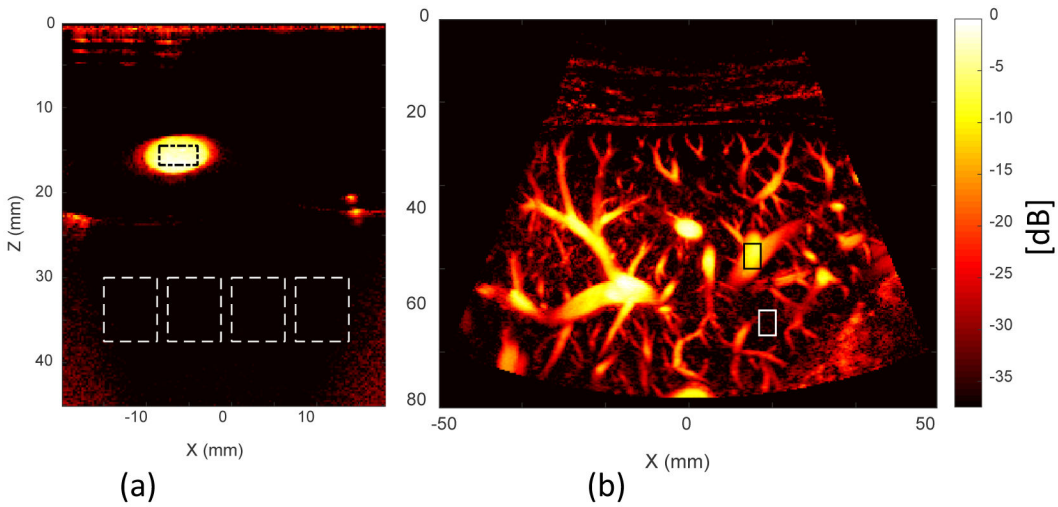

Fig.5.

(a) Blood flow phantom vascular image obtained with the proposed method, where incoherent clutter artifacts and background noise bias are greatly suppressed compared with Fig.1(a). The black rectangle indicates the blood flow ROI, and white rectangles denote the background ROIs for SNR estimation. (b) Human liver vascular image obtained with the proposed method. The contrast of the image is improved by the removal of noise bias and the incoherent clutter artifacts are suppressed compared to Fig 1(b). The black rectangle indicates a selected blood flow ROI, and the white rectangle denotes a background ROI for SNR estimation. Both images are displayed as a $10*\log_{10}()$ scale with the same dynamic range (−37.5 dB ~ 0 dB).

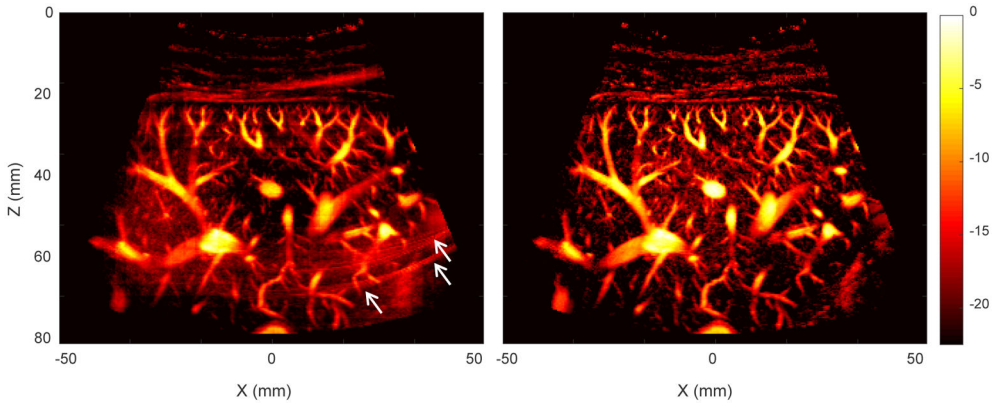

Fig.6.

(a) Liver vascular image obtained with the original block-wise local SVD filtering, where the side lobe artifacts cannot be completely removed, as indicated by the arrows. (b) Liver vascular image obtained with the combination of local SVD filtering and the proposed method, where both the noise and side lobe artifacts are greatly suppressed. Both images are displayed as a $10*\log_{10}()$ scale with the same dynamic range (−22.5 dB ~ 0 dB).

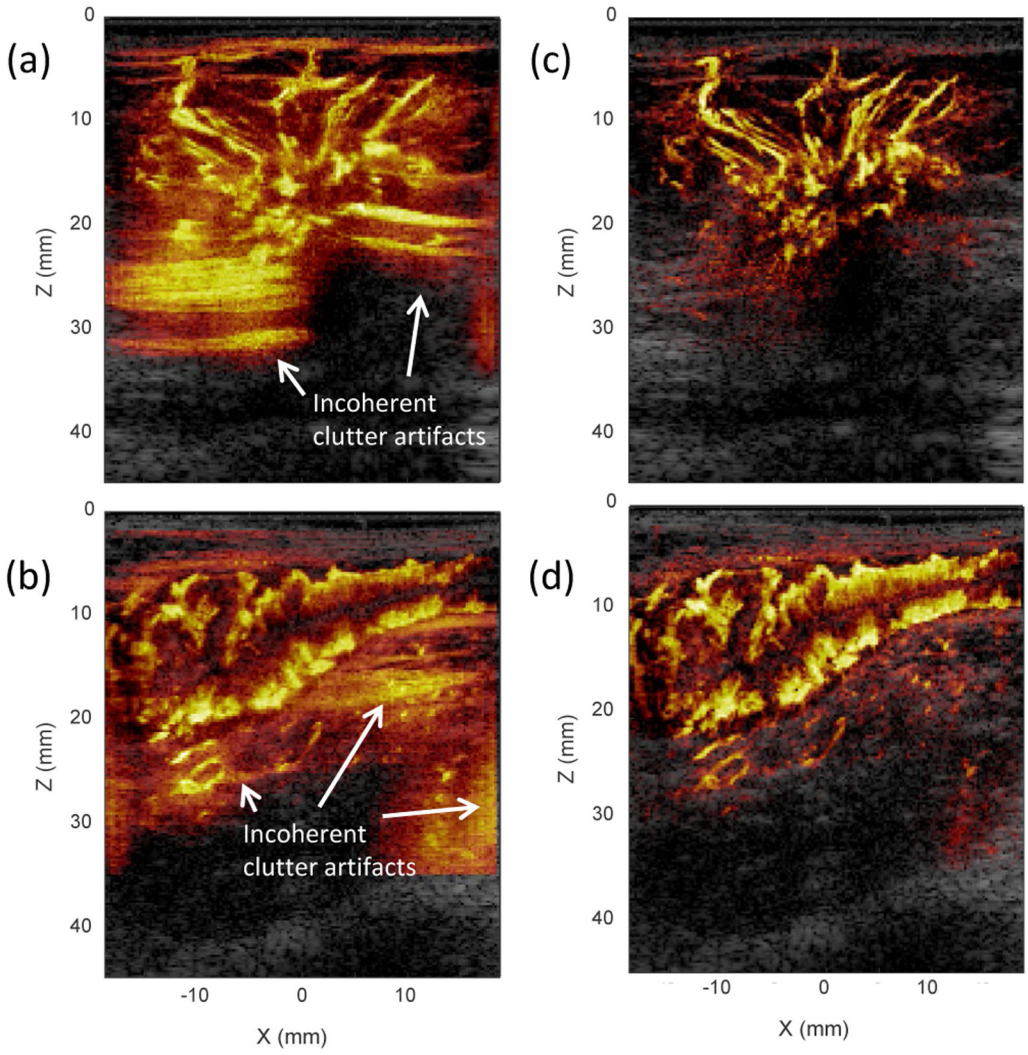

Fig. 7.

Ultrafast vascular images of (a) a breast tumor and (b) an inflammatory bowel segment filtered by the block-wise SVD filter without artifact suppression. Corresponding ultrafast vascular images of (c) the breast tumor and (d) the inflammatory bowel segment filtered by the block-wise SVD filter with artifact suppression using the proposed method. Vascular images are superimposed on the B-mode image for better visualization. All the vascular images are displayed as a $10*\log_{10}()$ scale with the same dynamic range (−25 dB ~ 0 dB).

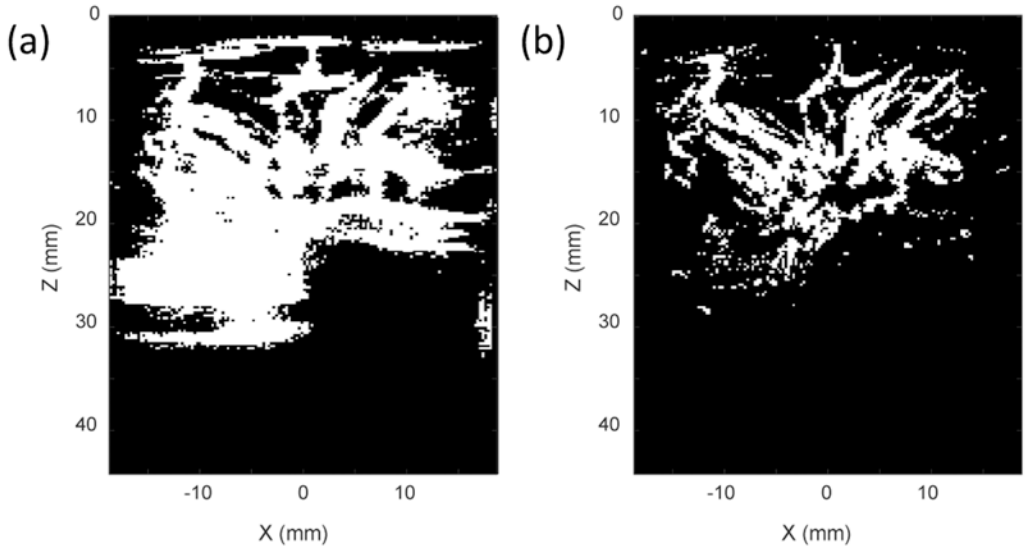

Fig. 8.

Binary images of breast tumor vascular images in Fig. 7(a) and 7(c), respectively, obtained by rejecting pixels below a threshold (−16 dB), which can be used for vessel area or vessel density estimation.

TABLE I

Imaging parameters for Ultrafast Vascular Imaging

settings	Linear array transducer (9L-D)	Curved array transducer C1-6-D
Transmission	Plane wave	Diverging wave
Number of transmitted angles	16	10
Angle increment (degree)	1	1
Receive F-number	0.69	0.69
PRF (kHz)	10	0.7143
Transmitted center frequency (MHz)	6.25	4.46
Post-compounded frame rate (Hz)	500	500
Ensemble	496	300
Number of pulse cycles	2	2
Image dimension (mm × mm)	44.5×37.5	80.4×102.8
Pixel size (mm × mm)	0.25×0.25	0.35×0.35
Block size (mm × mm) *	8.9×8.9	27.6×27.6
Block overlapping (%) *	90	95

* Block size and block overlapping are settings for block-wise adaptive SVD filtering only.